# SIMULATION OF STRESS-STRAIN STATE OF Zr1.0%Nb ALLOY DURING EQUAL-CHANNEL ANGULAR PRESSING: PART 2. STRESS DISTRIBUTION

H. ALSHEIKH[1], A. ROZHNOV[2], S. ROGACHEV[2], D. GRABCO[1,*], O. SHIKIMAKA[1]

[1] Institute of Applied Physics, Moldova State University, 5 Academy str., Chisinau, 2028, Republic of Moldova
*E-mails*: hanan.alsheikh@ifa.usm.md; daria.grabco@ifa.usm.md; olga.shikimaka@ifa.usm.md
[2] National University of Science and Technology MISIS, 4/1 Leninsky Prospekt, Moscow, 119049, Russia
*E-mail*: aeforscc@yahoo.com; csaap@mail.ru
[*]Corresponding author, E-mail: daria.grabco@ifa.usm.md; grabco@mail.ru

*Received October 2, 2024*

*Abstract:* Simulation of Zr1.0%Nb billet during equal channel angular pressing (ECAP) was conducted in QFORM program for one single pass at 420°C. The stress values, including mean stress $\sigma_m$, and equivalent stress $\sigma_{eq}$ along with their related area A% were calculated in the longitudinal (Y) and transverse (X) sections.

*Key words:* Zr1.0%Nb, ECAP simulation, stress distribution.

DOI: https://doi.org/10.59277/RomJPhys.2025.70.604

## 1. INTRODUCTION

Severe plastic deformation (SPD) is a powerful tool to produce bulk ultrafine grains and nanostructure materials [1]. SPD processes induce high compression stress in the materials along with high strain in a specified and restricted geometrical dimension without changing the material volume. Applying high compression stress suppresses crack initiation on the material surface and prevents material failure [2, 3]. Various methods exist for applying severe plastic deformation [4–9], such as equal channel angular pressing (ECAP), a repetitive process involving material deformation in two inclined channels with small geometrical dimensions [10]. Many studies [11–15] have discussed the application of additional back pressure to maintain the material under compressive stress throughout the entire process using both simulated and experimental methods. Additionally, the ECAP regime, which comprises factors such as: temperature, route (A, B, C), number of passes in channels, channel angle, arc of curvature (radius) in the lower die corner, deformation speed, mechanical properties of the material have a significant impact on the material failure during ECAP [16–20].

Therefore, an urgent demand has emerged for running a computational simulation of ECAP to select the optimal regime, which imposes a specific stress state on the material and prevents fracture to happen during high rate of deformation by applying various fracture criteria, as studied previously [21–25].

In this second part of our work (see the first part [26]), we investigate the mean and equivalent stress distribution in the longitudinal and transverse sections during the ECAP simulation for a single pass. This investigation allows to determine the channel, which induces the tensile stress on the billet, causing its fracture. Since, the absence of compressive stress on the material during severe plastic deformation initiate cracks on its surface, this can lead to material fracture in theses weak zones. Additionally, the equivalent stress values were calculated in these weak zones and compared to the ultimate tensile stress of Zr1.0%Nb alloy. This comparison is essential to determine the magnitude of tensile stress, which causing the billet fracture.

## 2. MATERIALS AND METHODS

The inputs data for simulation, which include the geometric parameters and the physical and chemical characteristics of the ECAP instrument and Zr1.0%Nb billet were discussed in detail in the first part of our study [26]. Here, a brief overview of the main steps of the research method is presented below.

*Simulation inputs.* In this work, we simulated the ECAP process for Zr1.0%Nb billet 110 mm long and 20 mm in diameter. Under real conditions, ECAP of Zr1.0%Nb billet is carried out in six passes. However, for this simulation, we simulated only the first ECAP pass under isothermal conditions at $T$ = 420°C. The channel angle was 108º, the strain rate was 0.21 $s^{-1}$, and the maximum pressing load was 0.3 mN.

The computational simulation of the thermal and stress-strain state was conducted in the QFORM program. The input data for the simulation includes:

– geometric dimensions of the ECAP die, punch, and billet;

– composition of the die, punch, and billet.

To build 3-D finite-element models of ECAP instrument and billet, Compass 3D program was used. Then the generation of finite elements meshes, and models assembling were carried out using QFORM program. The number of finite elements in the billet mesh was 46.795 elements, and 55.693 elements in ECAP instrument mesh.

*Geometrical dimensions, physical and chemical properties of the ECAP instrument and the billet*. To perform the simulation, data on the physical and mechanical properties of the billet and ECAP die were entered into the QFORM program. The data for Zr1.0%Nb billet were partially obtained from reference books (physical properties), and partially by conducting tensile and compressive

tests. The chemical composition of the Zr1.0%Nb alloy was as follows, in wt.%: (Nb 0.9 – 1.1; Fe 0.05; Ni 0.02; Al 0.008; Ti 0.005; C 0.02; Si 0.02; O 0.1; N 0.006).

The stress-strain curves obtained during mechanical tests were used for the simulation. Also, the mechanical characteristics of the Zr1.0%Nb alloy, including yield strength $\sigma_{0.2}$, ultimate tensile strength $\sigma_U$ and relative elongation at failure $\delta$, were derived from these curves and subsequently used in the simulation. The structure of as delivered Zr1.0% Nb alloy was partially recrystallized.

## 3. COMPUTATIONAL SIMULATION

*General algorithm of ECAP simulation*. QFORM program is capable of calculating the following values:

– temperature,
– strain,
– mean stress,
– equivalent stress.

Stress and material fracture depend mainly on the sign and the relationship of principal stresses $\sigma_1$, $\sigma_2$, and $\sigma_3$. The spherical tensor of these stresses is referred to as the mean stress $\sigma_m$, which is given by the formula:

$$\sigma_m = \frac{\sigma_1 + \sigma_2 + \sigma_3}{3}.$$

Mean stress indicates the volume changes in solids, and it acquires positive and negative values ($\sigma_m \leq 0$, or $\sigma_m \geq 0$). However, materials subjected to positive mean stress values are more prone to brittle fracture.

At the same time, stress deviator indicates the shape changes in the deformed solids. In this case, deviator is described by the equivalent stress, which is calculated using the following formula:

$$\sigma_{eq} = \sqrt{\sigma_1{}^2 + \sigma_2{}^2 + \sigma_3{}^2 - \sigma_1\sigma_2 - \sigma_2\sigma_3 - \sigma_3\sigma_1}.$$

Unlike the deviator $\sigma_m$, equivalent stress indicates volume unity and integrity, and it is considered a reduced stress, which equivalent to stress at plastic stage of uniaxial loading. This stress represents the same magnitude as would be induced under a multiaxial stress. Equivalent stress is used as strength criterion according to the energy theory and always acquires positive values [27]. The physical meaning of the equivalent stress presents the overall integral of the shear stress affecting the surrounding area of a point within the continuous material. Hence the shear stress relates to shape changes of each point of the continuous

material. Thus, the equivalent stress is defined as overall stress, arising due to the point distortion in the continuous material.

In this single-pass ECAP simulation, the values and sign of the mean stress (compressive (–), and tensile (+) stresses) arising in the channels of ECAP die were calculated in both the longitudinal and transverse sections of the Zr1.0% Nb billet. Additionally, fracture criterion was applied by calculating the equivalent stress values in different sections, to determine the crack initiation zones on the billet surface within the die channels.

The methods used for selecting the upper and lower surfaces during ECAP process, as well as the longitudinal (Y) and transverse (X) sections, the positions of the transverse sections X within the channels (A, B, C, D, E), the moments $t_i$ (or stages) of deformation within the deformation zones (intersection channels), and the designation of selected sections at specific deformation moments ($Y(t_i)$, $X(t_i)$) were illustrated and discussed thoroughly in the first part of our work [26].

## 4. RESULTS AND DISCUSSION

### 4.1. MEAN STRESS DISTRIBUTION

Figure 1 illustrates the inhomogeneity of stress distribution along the longitudinal sections $Y(t_i)$, where $i = 1, 2, 3$, at various deformation moments. After one pass, the stress values in these sections can be categorized into six mean stress groups:

– group 1: tensile stress ($100 < \sigma_m < 200$) MPa,
– group 2: tensile stress ($0 < \sigma_m < 100$) MPa,
– group 3: compressive stress ($0 > \sigma_m > -100$) MPa,
– group 4: compressive stress ($-100 > \sigma_m > -200$) MPa,
– group 5: compressive stress ($-200 > \sigma_m > -300$) MPa,
– group 6: compressive stress ($-300 > \sigma_m > -800$) MPa.

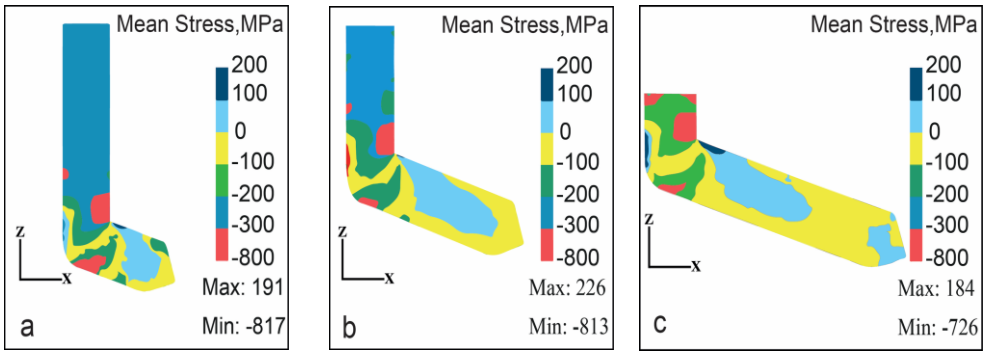


Fig. 1 – Stress distribution along longitudinal sections: a – $Y(t_1)$, b – $Y(t_2)$, c – $Y(t_3)$.

Table 1 presents the positions, value ranges, and related area *A*[%] of the stress groups in the longitudinal sections. The results reveal that area *A*[%] of stress groups 1, 4, 6 remains constant and relatively small during all moments of deformations. The zones occupied by these groups on the distribution maps are located along one of the surfaces within the intersection channels (deformation zones). Conversely, the area *A*% of stress group 3, which occupies zones on the billet within the exit channel, increases by 14, 28, 31 % at $t_1$, $t_2$, $t_3$, respectively. This increase in area correlates with passing the billet in the intersection channel at $t_i$, and by a decrease in area *A*[%] of zones occupied by stress group 5 on the billet within the entry channel.

*Table 1*

Positions and Area [%] of mean stress groups

| Stress | | | | | | Area *A*[%] | | |
|---|---|---|---|---|---|---|---|---|
| Stress group | Zone color | Zone position | Surface | Stress value σ [MPa] | Stress | Longitudinal sections Y($t_i$) | | |
| | | | | | | Y($t_1$) | Y($t_2$) | Y($t_3$) |
| 1 | Sea paint blue | Intersection channel | Upper (exit)–lower (entry) | $100 < \sigma_m < 200$ | Tension | 0.4 | 0.4 | 0.4 |
| 2 | Blue Mana | Exit channel | Exit | $0 < \sigma_m < 100$ | Tension | 11 | 22 | 22 |
| 3 | Yellow | Exit channel – Intersection channels | Upper (exit) Lower (entry) | $0 > \sigma_m > -100$ | Compression | 14 | 28 | 31 |
| 4 | Green | Intersection channel | Upper –lower | $-100 > \sigma_m > -200$ | Compression | 10 | 8 | 9 |
| 5 | Sea Dream blue | Entry channel | – | $-200 > \sigma_0 > -300$ | Compression | 59 | 35 | 10 |
| 6 | Red | Intersection channels | Upper (entry) Lower (exit) | $-300 > \sigma_0 > -800$ | Compression | 6 | 4 | 5 |

However, the area *A*[%] of tensile stress group 2 on the upper surface in the exit channel increases from 11 to 22% at $t_2$, and then remains constant at 22% at $t_3$ due to the billet extraction from the die. This transition from negative compressive mean stress in the entry channel to a positive tensile mean stress in the exit channel could initiate cracks on the upper surface of the billet leading to fracture because of insufficient plasticity [28].

Figure 2 illustrates the stress distribution map of the section *A*($t_1$) within the entry channel. Stress group 5 occupies the entire area of this section. So, the billet in this channel subjects to a compressive stress ($-200 > \sigma_0 > -300$ MPa).

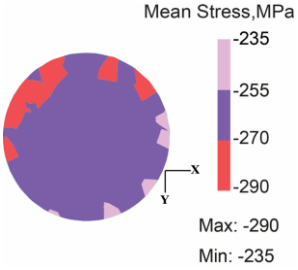


Fig. 2 – Mean stress distribution in section $A(t_1)$.

Figure 3 illustrates the stress distribution map of the section $B(t_i)$ within the entry channel, where the compressive stress groups 3, 4, 5, and 6 covers 33, 38, 27, 2% in $B(t_1)$, 33, 33, 29, 6% in $B(t_2)$, 41, 25, 29, 4% in $B(t_3)$. Hence, all sections in the entry channel subject to compressive stress ($0 > \sigma_0 > -800$ MPa).

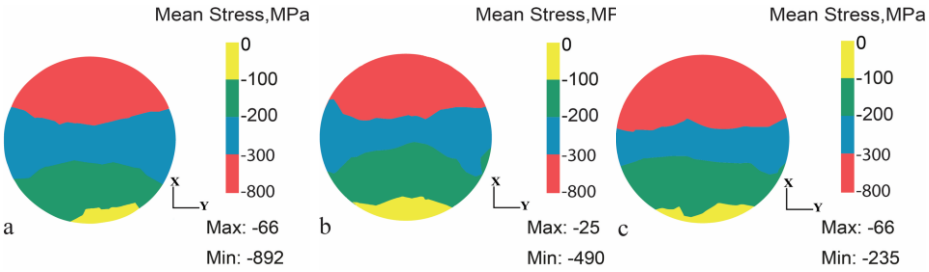


Fig. 3 – Mean stress distribution in sections: a – $B(t_1)$, b – $B(t_2)$, c – $B(t_3)$.

However, this variation in stress distribution in sections $B(t_i)$ appears due to billet approaching the shearing zone (intersection channel). In the deformation zone (intersection channels), as illustrated in Fig. 4, a similar variation in stress distribution is detected in sections $C(t_i)$, accompanied by an increase in the stress area of groups 5, and 6 on the lower surface of the billet. In the shearing plane the compressive stress of groups 3, 4, 5, and 6 ($0 > \sigma_0 > -800$ MPa) covers 9, 15, 51, 25% in $C(t_1)$, 4, 14, 50, 31% in $C(t_2)$, 9, 18, 44, 29% in $C(t_3)$.

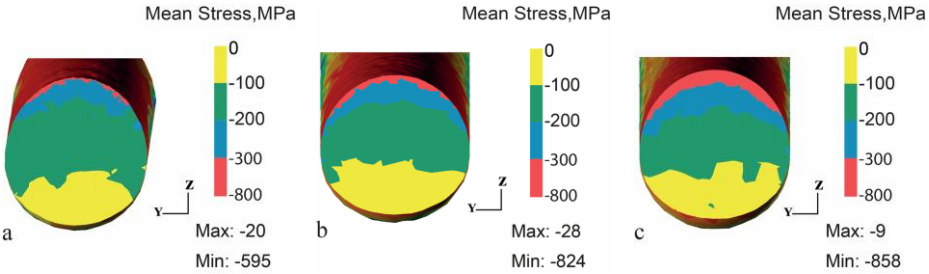


Fig. 4 – Mean stress distribution in sections: a – $C(t_1)$, b – $C(t_2)$, c – $C(t_3)$.

This variation in stress during shearing deformation in sections $B(t_i)$ and $C(t_i)$ is attributed to the mechanical properties of the metallic billet. As the stress variation is related to the arc of curvature of the billet on the lower corner of the die, and the gap between the billet and the die. So, the stress in this surface deviate from simple shear to a more complex shear. As the billet passes through the deformation zone, a transition is observed on the upper surface from compressive stress groups 3, and 4 ($0 > \sigma_m > -200$) MPa to tensile stress groups 1, and 2 ($0 < \sigma_m \leq 200$ MPa). The tensile stress covers 19, 17, 15 % of sections $D(t_1)$, $D(t_2)$, and $D(t_3)$ as illustrated in the Fig. 5, while the lower zone remains under compressive stress of groups 3, and 4 covering 25, 50 % in $D(t_1)$, 21, 53 % in $D(t_2)$, and 28, 52 % in $D(t_3)$.

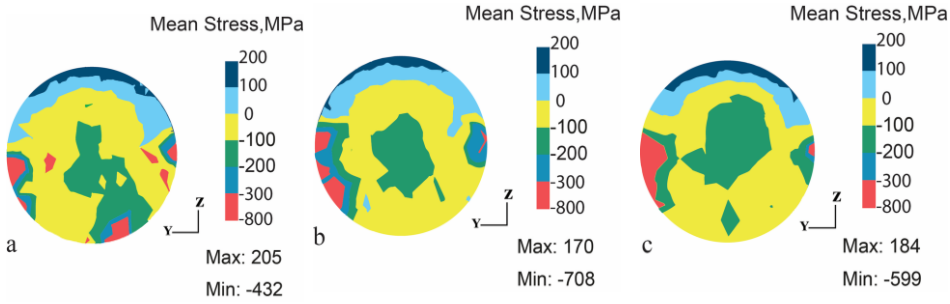


Fig. 5 – Mean Stress distribution in sections: a – $D(t_1)$, b – $D(t_2)$, c – $D(t_3)$.

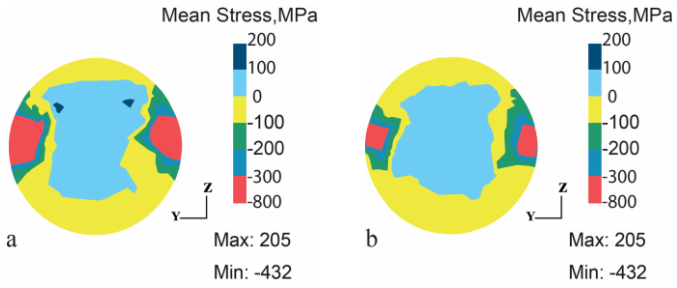


Fig. 6 – Mean stress distribution in sections: a – $E(t_2)$, b – $E(t_3)$.

After one single pass in ECAP die, the stress distribution in sections $E(t_2)$, and $E(t_3)$ exhibits two principal zones (Fig. 6): central tensile stress of group 2 covering 40, and 41% of the area in $E(t_2)$, and $E(t_3)$, respectively, and the compressive stress of group 3 on the upper and lower surfaces covering 39, 45% of the area in $E(t_2)$, and $E(t_3)$, respectively.

### 4.2. EQUIVALENT STRESS DISTRIBUTION

Figure 7 shows that the equivalent stress begins to increase from 350 to 400 MPa on the upper surface after shearing deformation in the intersection

channels, this increase in stress occupies an area of 24, 49, 75% in $Y(t_1)$, $Y(t_2)$, and $Y(t_3)$, respectively.

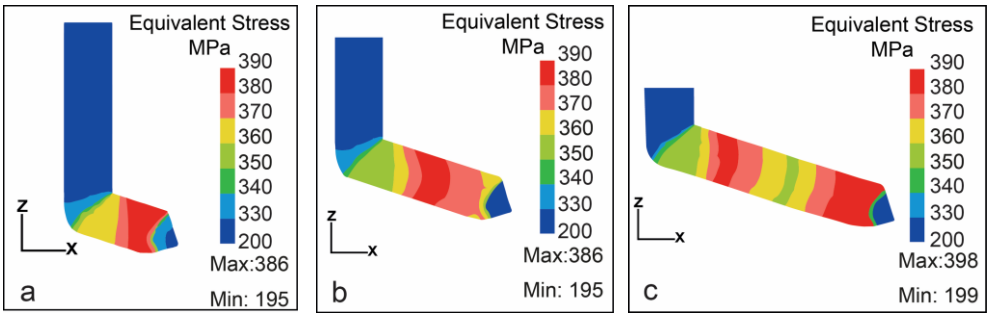


Fig. 7 – Equivalent stress distribution along longitudinal sections: a – $Y(t_1)$, b – $Y(t_2)$, c – $Y(t_3)$.

Figure 8 illustrates that the equivalent stress remains constant at 199 MPa in sections $A(t_1)$, $B(t_1)$, $B(t_2)$, and $B(t_3)$ before entering the deformation zone. Figure 9 illustrates a slight increase in equivalent stress to 350 MPa in the deformation zone, especially in the central zones of the sections $C(t_i)$. The area of these central zones covers 66, 56, 60 % in sections $C(t_1)$, $C(t_2)$, and $C(t_3)$, respectively.

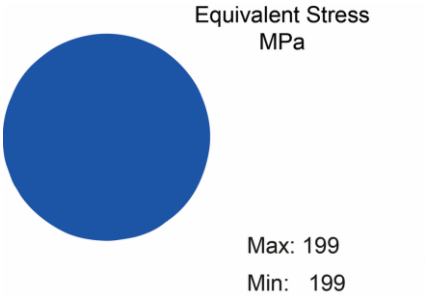


Fig. 8 – Equivalent stress distribution in sections $A(t_1)$, $B(t_1)$, $B(t_2)$, and $B(t_3)$.

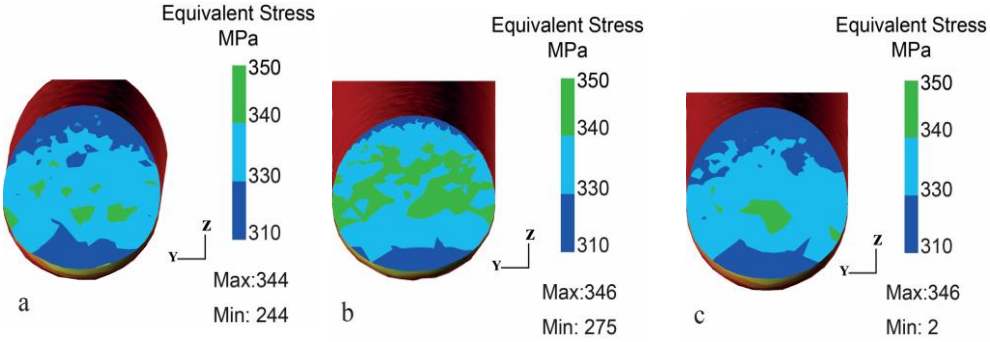


Fig. 9 – Equivalent stress distribution in sections: a – $C(t_1)$, b – $C(t_2)$, c – $C(t_3)$.

Figure 10 illustrates an increase in equivalent stress on the upper surface of the billet in the exit channel, rising from 360 to 370 MPa. This increase covers 45, 9, 48 % in sections $D(t_1)$, $D(t_2)$, and $D(t_3)$ respectively. The high equivalent stress on the upper surface correlates with the transition of mean stress from compressive to tensile as shown in Fig. 5. At steady state of deformation ($t_2$) the equivalent stress increase has the minimum values among sections.

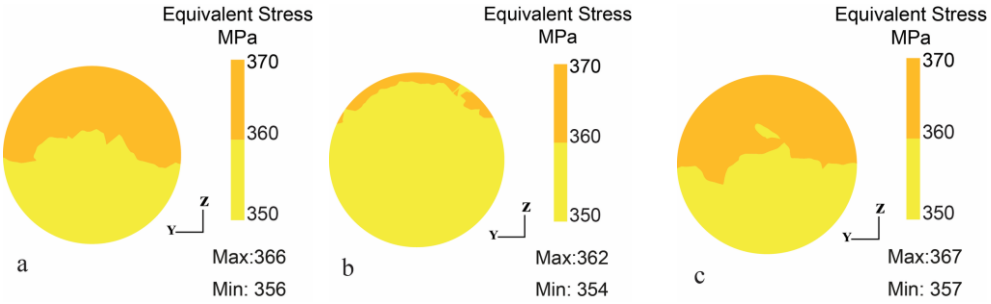


Fig. 10 – Equivalent stress distribution in sections: a – $D(t_1)$, b – $D(t_2)$, c – $D(t_3)$.

After one single pass in ECAP die, the equivalent stress continues to rise, reaching a maximum value of 380 MPa. The area of these high stress zones covers 64, 52 % in $E(t_2)$, and $E(t_3)$ respectively as illustrated in Fig. 11. The initiation of cracks on the upper surface of Zr1.0%Nb billet in the exit channel is unlikely, as the maximum equivalent stress on this surface is below the ultimate tensile strength.

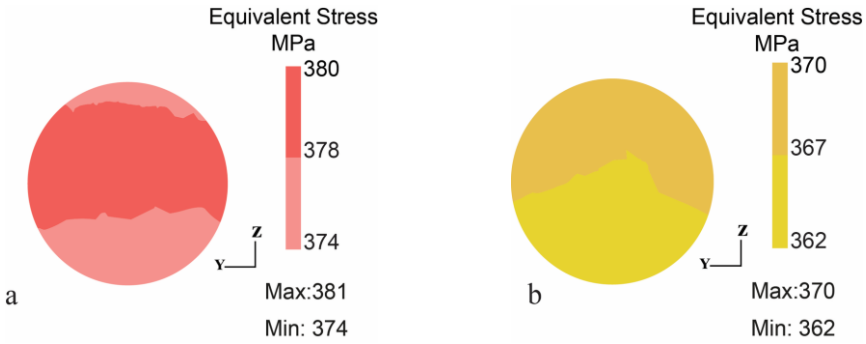


Fig. 11 – Equivalent stress distribution in sections: a – $E(t_2)$, b – $E(t_3)$.

However, the simultaneous presence of compressive and tensile stress in one section ($d$ = 20 mm) with relatively high equivalent stress leads to a variation in microstructural size, which has a negative effect on the mechanical properties of Zr1.0%Nb.

### 4.3. INTERRELATION OF BILLET PHYSICAL PARAMETERS IN ECAP

In general, the results obtained in this study on stress distribution in zirconium alloy during ECAP are a continuation and inextricably linked to the strain and temperature distribution previously investigated in our earlier works [26, 29]. The calculations revealed the following evolution of stress, strain, and temperature distribution in the Zr1.0%Nb billet during ECAP. Applying an external load on the billet within the entry channel (transverse section $A(t_1)$), the billet is subjected to compressive stress ranging from ($-200 > \sigma_0 > -300$ MPa). As the billet moves straightforward, the compressive stress increases throughout the entire sample, reaching its maximum value in sections $B(t_i)$ and $C(t_i)$ ($0 > \sigma_0 > -800$MPa).

However, the billet remains undeformed in the entry channel until it approaches the deformation zone, where the temperature of the billet increases in the channel intersection zone, or shearing deformation zone, to 430°C, which exceeds the initial temperature of 420°C by approximately 10°C. Thus, the shear deformation zone acts as a heat source due to high induced plastic deformation in this zone. However, such an increase in temperature is insignificant to affect ECAP process. For instance, the billet temperature rose by 250°C due to an increase in the deformation rate from 0.264 $s^{-1}$ to 21.4 $s^{-1}$ [22]. Additionally, the authors point out, that a thermal rise within the deformation zone up to 70°C has no negative influence on the ultrafine-grained (UFG) structure of the processed material. Within the deformation zone, the high imposed strain deviates from simple shear to a more complex stress state, leading to microstructural fragmentation through inhomogeneous deformation in different parts of the billet. This indicates that the channel intersection (or shearing deformation zone) represents the area, where the most pronounced grain refinement occurs, accompanied by both micro- and nano-fragmentation of grains. However, this inhomogeneous refinement can be minimized to an acceptable level by rotating the billet by 90° or increasing the number of passes to six.

Figure 12 illustrates the grain refinement in Zr1.0%Nb from 1.5 μm to 0.5 μm, with the interior zone containing structural elements, such as fragments, and subgrains with sizes down to 122 nm. Within the exit channel, after shearing deformation, a transition is observed on the upper surface from compressive stress ($0 > \sigma_m > -200$ MPa) to tensile stress ($0 < \sigma_m \leq 200$ MPa). Concurrently, the billet temperature decreases to 380°C by forming a temperature gradient along its length. Just before billet extraction, the stress distribution in sections $E(t_2)$ and $E(t_3)$ shows two zones: the central tensile stress and the compressive stress on the upper and lower surfaces.

A similar result was obtained in [23], where the effect of a modified die on the deformation distribution in the Al6060 alloy subjected to ECAP was investigated using the finite element method. The authors found that a conventional ECAP die induces tensile stress on the upper surface of the sample, particularly within intense

plastic deformation zone, increasing the tendency for cracking and failure of the sample and complicating further ECAP processing. Whereas the modified ECAP die shifts the stress state from tension to compression.

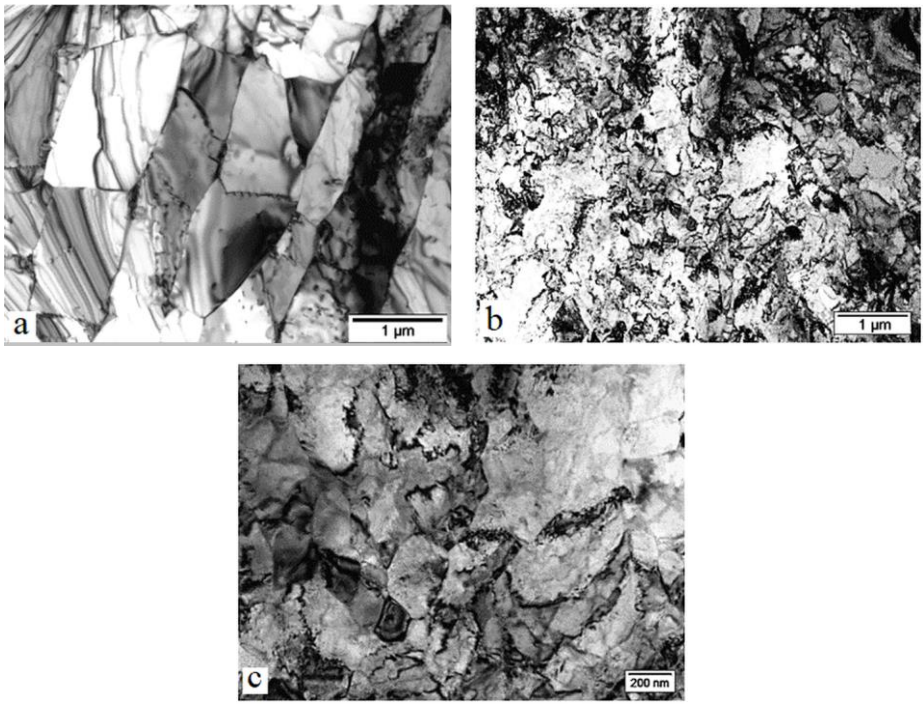


Fig. 12 – Microstructure of Zr1.0%Nb alloy before ECAP (a) and after ECAP (b, c).

The material behavior and strain distribution of a commercially pure titanium (CP-Ti) sample were investigated previously [24]. The simulation results also showed that tensile stress occurs near the upper surface of the processed sample, which makes the workpiece prone to cracking and failure. The authors of [25] also found that tensile stress increases the sample's tendency to cracking and failure and complicates further ECAP processing. Therefore, in order to reduce the tendency to cracking and failure, the application of back-pressure was proposed in these works.

Thus, these studies and literature data point out, that ECAP method is a complex, multi-level process for forming ultrafine-grained structures, causing a significant change in material properties.

## 5. CONCLUSIONS

ECAP simulation of Zr1.0%Nb billet was performed in QFORM program for a single pass at temperature 420°C. Mean and equivalent stress distribution

maps were calculated for both the longitudinal and transverse sections. Additionally, the area of the detected zones on these maps was calculated. It was established that:

– within the intersection channel (deformation zone), compressive stress variation is observed on the upper and lower surface, while the central zone primarily subjects to shearing stress ($-100 > \sigma_m > -200$);

– after passing the deformation zone, a stress transition from compression to tensile is detected on the upper surface of the billet within the exit channel. This transition correlates with an increase in equivalent stress, reaching a maximum of 380 MPa;

– after one pass of the billet in channels, no cracks are expected on the upper surface of the Zr1.0% Nb billet, as the maximum equivalent stress on this surface is below the ultimate tensile strength (420.5 MPa). However, a heterogeneous structural distribution with varying microstructural element sizes is anticipated.

*Acknowledgements.* This study was supported by the research Subprogram **011201** of the Institute of Applied Physics, State University of Moldova, funded by the Ministry of Education and Scientific Research of Moldova Republic.

REFERENCES

1. Kapoor, R., Chapter 20, 2017, in: *Materials under Extreme Conditions*, Elsevier Inc., pp. 717–754. doi:10.1016/B978-0-12-801300-7.00020-6.
2. E.M. Zayed, M. Shazly, A. El-Sabbagh and N.A. El-Mahallawy, Heliyon **9**(6), e16700 (2023). https://doi.org/10.1016/j.heliyon.2023.e16700
3. R.N. Harsha, V.M. Kulkarni and B. Satish Babu, Materials Today: Proceedings **5**, 22340–22349 (2018). https://doi.org/10.1016/j.matpr.2018.06.600
4. K. Mohan Agarwal, A. Singhal, A. Kapoor and D. Bhatia, Mater. Sci. Energy Technol **4**, 290–295 (2021). https://doi.org/10.1016/j.mset.2021.08.005
5. A. Hohenwarter and S. Wurster, J. Mater. Sci. **59**, 6048–6058 (2024). https://doi.org/10.1007/s10853-023-09147-2
6. L. Ou, L. yan Li, C. he Fan, Y. feng Nie, and J. jun Yang, Transactions of Nonferrous Metals Society of China **33**, 2001–2013 (2023). https://doi.org/10.1016/S1003-6326(23)66239-9
7. S. Öğüt, H. Kaya, A. Kentli, K. Özbeyaz, M. Şahbaz and M. Uçar, Archives of Metallurgy and Materials **66**, 431–436 (2021). https://doi.org/10.24425/amm.2021.135875
8. A.Volokitin, A. Naizabekov, I. Volokitina, S. Lezhnev and E. Panin, Mater. Lett. **304** (2021). https://doi.org/10.17632/6m5r6f2z5g.1
9. P. Bereczki, G. Krallics and J. Renkó, Procedia Manufacturing **37**, 253–260 (2019). https://doi.org/10.1016/j.promfg.2019.12.044
10. R.Z. Valiev, R.K. Islamgaliev and I.V. Alexandrov, Progress in Mater. Sci. **45**, 103-189 (2000). https://doi.org/10.1016/S0079-6425(99)00007-9
11. R.Y. Lapovok, J. Mat. Sci. **40**, 341–346 (2005). https://doi.org/10.1007/s10853-005-6088-0
12. P.W.J. Mckenzie and R. Lapovok, Acta Mater. **58**, 3198–3211 (2010). https://doi.org/10.1016/j.actamat.2010.01.038
13. N. Sadasivan, S. Madhu and M. Balasubramanian, Mater. Today: Proceedings **22**, 1228–1232 (2020). https://doi.org/10.1016/j.matpr.2019.11.332
14. N. Singh and M. Kumar Agrawal, MATEC Web of Conf. **392**, 01030 (2024). https://doi.org/10.1051/matecconf/202439201030

15. A. Panigrahi, N. Scheerbaum, P. Chekhonin, J. Scharnweber, B. Beausir, M. Hockauf, S. Sankaran and W. Skrotzki, IOP Conf. Series: Materials Science and Engineering **63**, 012153 (2014). doi:10.1088/1757-899X/63/1/012153
16. J. Gao, T. He, Y. Huo, T. Yao and H. Hong, Procedia Manufacturing **50**, 119–124 (2020). https://doi.org/10.1016/j.promfg.2020.08.022
17. S.W. Chung, W.-J. Kim, M. Kohzu and K. Higashi, The Process Simulation **44**, 973-980 (2003). https://doi.org/10.2320/matertrans.44.973
18. L. Shekher Jabur, Intern. J. of Scientific Eng. & Sci. **4**, *8*, 24-28 (2020).
19. J. Wang, Z. Li and C. Ma, J. of Physics: Conference Series **1678**, 012035 (2020). doi:10.1088/1742-6596/1678/1/012035
20. A. Gupta, K. K. Saxena, A. Bharti, J. Lade, K. Chadha and P.R. Paresi, Advances in Materials and Processing Technologies **8**, 1635–1646 (2022). https://doi.org/10.1080/2374068X.2021.1953917
21. A. I. Alateyah, M. M. Z. Ahmed, Y. Zedan, H. Abd El-Hafez, M.O. Alawad and W.H. El-Garaihy, Metals **11**, 607 (2021). https://doi.org/10.3390/met11040607
22. R. Asfandiyarov, D. Aksenov and G. Raab, Intern. Scientific Journal: Machines. Technologies. Materials **14**, (6), 237–239 (2020).
23. M.A. González-Lozano, P. Ponce-Peña, M.A. Escobedo-Bretado, R.H. Lara-Castro, and B.X. Ochoa-Salazar, MRS Advances **1818**, 13–19 (2015). https://doi.org/10.1557/opl.201.680
24. T. Horn, C. Silbermann and J. Ihlemann, PAMM: Proc. Appl. Math. Mech. **17**, 309–310 (2017). DOI 10.1002/pamm.201710124
25. A. Shahira Kamaruddin and M.N. Katimon, Research Progress in Mechanical and Manufacturing Engineering **2**, 433–441 (2021). https://doi.org/10.30880/rpmme.2021.02.02.049
26. H. Alsheikh, A.B. Rozhnov, S.O. Rogachev, D.Z. Grabco and O.A. Shikimaka, Rom. J. Phys. **69**, 617 (2024).
27. L.B. Potapova and V.P. Yartsev, Moscow: Mashinostroenie (in Russian), 2005, 244 p.
28. S.C. Yoon, C.H. Bok, M.H. Seo, T.S. Kim and H.S. Kim, Mater Trans. **49**, 963–966 (2008). doi:10.2320/matertrans.MC200723
29. H. Alsheikh, A.B. Rozhnov, S.O. Rogachev, D.Z. Grabco and O.A. Shikimaka, Electronic Mater. Processing (in Russian) **5** (2024); Surf. Eng. Appl. Electrochem **6** (2024), in press.